

Microstructural analysis of geopolymers using fused slags with transmission electron microscopy

Yootaek Kim* and Kyongwoo Lee

Department of Materials Engineering, Kyonggi University, Suwon 463-760, Korea

The amount of fused slag generated is continuously increasing and is expected to reach 50,000 tons per year as coal gasification facilities and waste treatment systems producing fused slag have been actively adopted recently in Korea. One of the prospective solutions is to make geopolymers with the slags because geopolymers are a cement substitute that can reduce the generation of carbon dioxide and have thus attracted increasing interest from recycling and eco-friendly construction industries because they provide sufficient mechanical strength for application in construction materials. There has not yet been a comprehensive microscopic investigation of geopolymers or diffraction pattern analysis of the crystallites produced by geopolymerization. Geopolymers made of fused slags with an alkali activator exhibited very high compressive strength compared with those of ordinary geopolymers, and their microscopic structures were analyzed by transmission electron microscopy (TEM) to confirm the formation of crystallites during the geopolymerization and to explain the relationship between the microstructure and mechanical property of the geopolymers. At least two types of phases, C-S-H and Ca(OH)₂, have been identified by selected area diffraction (SAD) pattern analyses on the crystallites in the geopolymer matrix.

Key words: Fused slag, Geopolymer, Microstructure, Si/Al ratio, TEM.

Nomenclature

C-S-H = calcium silicate hydrate
C-A-H = calcium aluminum hydrate

Introduction

Many studies have recently focused on environment-friendly construction materials, which produce less carbon dioxide resulting in the reduction of CO₂ emissions. Moreover, low-grade coal has become a major energy source as energy consumption increases because it is abundant and inexpensive. Recently, many integrated gasification combined cycle (IGCC) process facilities were built in Korea in accordance with the policy of energy diversification. The recycling of wastes such as fused slags produced from the IGCC process and municipal solid waste incinerator fly ash has also been performed to increase the recycling rate and protect the environment to catch up with the increasing social needs resulting from the rapid increase in the amount of fused slags from various fields [1, 2]. One of the solutions is to use geopolymers, which are a type of inorganic and polymeric material and are a prospective alternative to ordinary Portland cement (OPC) [3,4]. It has been reported that geopolymer-based concrete releases only 1/6 of the CO₂ emitted by the production of OPC

[5, 6].

The geopolymerization reaction is exothermic and results in the formation of compact, amorphous to semi-crystalline solid materials. Therefore, geopolymers are inorganic polymers, which are macromolecules linked by covalent bonds that have a-Si-O-M-O-backbone, where M usually denotes aluminum [7-9]. It is well known that the Si/Al ratio of geopolymer binders strongly affects the resulting properties [10]. It is expected that the compressive strength of geopolymers should increase monotonically with the silica content because the strength of Si-O-Si bonds is higher than those of Si-O-Al and Al-O-Al bonds [11, 12].

The fused slag (FS) used in this study was obtained from the fused slag (melted residues) after gasification processes. The other type of slag used in this study is called spent catalyst slag (SCS), which was produced as a by-product during the extraction of precious metals from spent catalysts.

Phase analyses of geopolymers using techniques including X-ray diffraction (XRD), infra-red (IR) spectroscopy, and Raman spectroscopy have been performed by many researchers; the phases among geopolymers, OPC, blast furnace slag, and alkali-activated slag have been compared, some of the peaks have been indexed, suggesting the existence of crystallites in the matrix of geopolymers [13-16]. Some papers have also suggested the existence of crystallites in the matrix of geopolymers based on scanning electron microscopy (SEM) and energy dispersive spectroscopy (EDS) analysis only [3, 17-19]. However, crystal structural analyses using electron

*Corresponding author:
Tel : +82-31-249-9765
Fax: +82-31-249-9774
E-mail: ytkim@kgu.ac.kr

diffraction patterns obtained from crystallites in the matrix of geopolymers have been rarely reported by other researchers [13]. Phase changes or new phases after high-temperature treatment of geopolymers have been reported; however, few researchers have reported the creation of crystalline phases during the geopolymerization process at low-temperature curing [20-22].

In this study, SAD patterns from a geopolymer matrix were indexed, and it was also speculated that the mechanical property is related to the Si/Al ratio as well as the existence of micro-crystallites in the geopolymer matrix.

Methodology

The Si/Al ratio was controlled by mixing two fused slags with different compositions, as observed in Table 1, FS were obtained after the melting-gasification process during the combustion of urban municipal solid waste, and sewage sludge was obtained by feeding cooling water at room temperature. SCS was produced as a by-product during the extraction of precious metals from spent catalysts at high temperature. FS and SCS were milled for 2 hrs to obtain particles that were then passed through a 106 mesh sieve. The compositions in Table 1 were determined using X-ray fluorescence (XRF; SPECTRO 2000). The FS and SCS were mainly composed of silica, alumina, and calcia but with different contents.

XRD analyses of the two slags in Table 1 have been reported earlier [24]; the phases of both FS and SCS are completely amorphous; no particular peak and only background was observed, which is typical for XRD patterns from amorphous materials. SEM examination reveals that the particle size and shape of FS and SCS

Table 1. Compositions (wt.%) of the FS and SCS used for the production of geopolymers with different Si/Al ratios. The Si/Al ratio was controlled by mixing FS and SCS in the proportions listed in Table. 2.

Oxide	FS	SCS
SiO ₂	47.26	29.71
Al ₂ O ₃	17.70	35.81
Fe ₂ O ₃	7.61	0.64
CaO	11.83	22.66
MgO	3.00	7.75
Na ₂ O	3.26	0.18
K ₂ O	1.50	0.34
TiO ₂	0.78	0.4
ZrO ₂	–	1.96
P ₂ O ₅	–	0.5
Cr ₂ O ₃	1.40	–
MnO	–	–
SO ₃	0.12	–
Si/Al	2.27	0.70

Table 2. FS/SCS mixing ratios and resulting Si/Al ratios of the geopolymers.

FS : SCS	Si/Al ratio
100 : 0	2.27
80 : 20	1.74
60 : 40	1.37
40 : 60	1.09
20 : 80	0.88
0 : 100	0.7

were similar, and the particle size distribution of each raw material was also similar [23]; it is well know that the particle size distribution is one of the main influencing factors on geopolymerization [24, 25]. Therefore, the effect of the particle size distribution of raw materials on the compressive strength of geopolymers may be negligible.

The liquid/solid ratio was fixed at 0.15. Pellets, 10 mm in both diameter and height, were prepared by compression molding at a pressure of 25 MPa for 20 sec. For curing, the specimens were sealed in a polyethylene zipper bag to prevent the evaporation of moisture; the internal humidity was maintained at 99%.

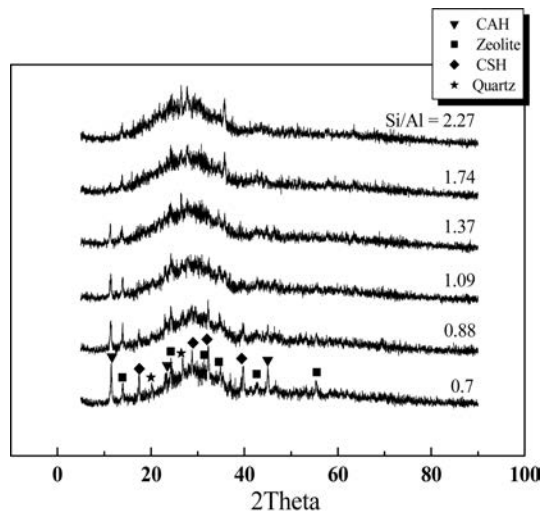
The compressive strength of the cylindrical geopolymer pellets was determined using a universal test machine (UTM; UTM-900NH Series, DAEKYUNG, Korea) at a crosshead speed of 5 cm/min. The phase analysis was performed using XRD (XRD; MiniFlex2, Rigaku, Japan), which was operated at 40 kV and 40 mA using Cu-K_α radiation. The microstructure of the geopolymers was observed by SEM (S-4800, HITACHI, Japan) using secondary electrons and by TEM (JEM-3010, JEOL Japan). The specimens were coated with platinum before the SEM observations at an accelerating voltage of 5 kV. The TEM specimens were milled using an ion-miller (Quanta 3D FEG, FEI, USA) and mounted on a platinum grid.

Results and Discussion

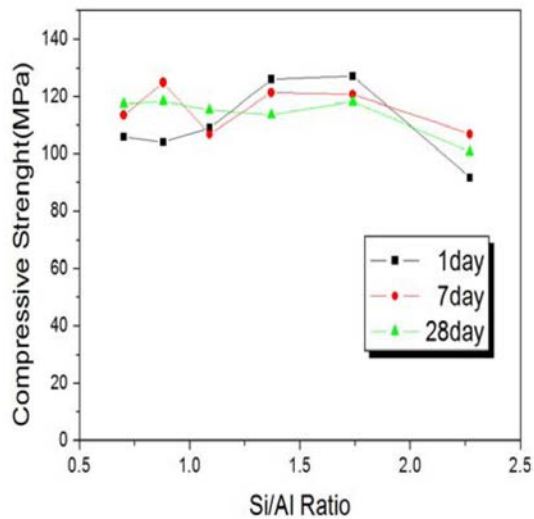
XRD analysis and compressive strength

Fig. 1(a) shows the XRD peaks from geopolymers with six different Si/Al ratios after geopolymerization. C-S-H (calcium silicate hydrate), C-A-H (calcium aluminum hydrate), zeolite, and quartz peaks are identified. Some crystalline phases formed in all of the specimens from the completely amorphous phase after geopolymerization. The degree of crystallinity can hardly be determined by XRD analyses; however, it appears that the number of diffraction peaks and intensities increased with decreasing Si/Al ratio. The C-A-H and zeolite peaks are almost disappeared at high Si/Al ratio.

Fig. 1(b) shows the compressive strengths of the geopolymers after three different aging periods. The compressive strength of all the specimens of this study is much higher than that of ordinary geopolymers made



(a)

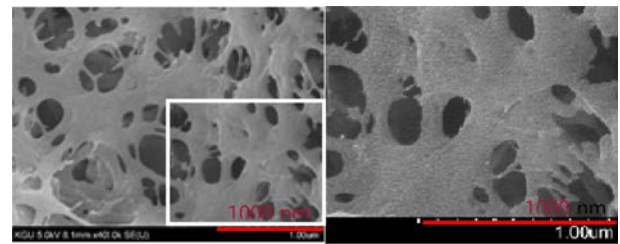


(b)

Fig. 1. (a) XRD patterns of the geopolymers with 6 different Si/Al ratios after geopolymerization and (b) compressive strength of geopolymers with 6 Si/Al ratios for 1, 7, and 28 days of aging.

of metakaoline or related materials [5, 12]. It should be noted that the specimens in this study were prepared using pressure molding (25 MPa for 20 sec), a low liquid/solid ratio (0.15 for solid/liquid), and a high alkali concentration (18 M), which may explain the relatively high compressive strength compared with that of ordinary geopolymers. However, investigating the effects of the Si/Al ratio and of emerging new phase(s) after geopolymerization on the compressive strength of geopolymers under the above experimental conditions remains of interest.

The compressive strength during the early stage of curing (1 day and 7 days) was even slightly higher than that after a longer curing period of 28 days, although



(a)

(b)

Fig. 2. SEM micrographs from the geopolymer with a Si/Al ratio of 1.74 after 28 days of aging. (a) A lower magnification image shows a smooth matrix. (b) A higher magnification image of the boxed region in (a) shows many micro-crystallites in the matrix as well as in the network structure between the matrices.

the difference was within 20 MPa. Hence, only a slight change in the compressive strength of the specimens was observed after 28 days of curing. Therefore, it can be concluded that the Si/Al ratio affects the compressive strength during the early stage of curing, whereas there is almost no effect on the compressive strength at the longer stage of curing.

SEM analysis

It was previously reported that the compressive strength of geopolymers made of FS and SCS is closely related to the microstructure of the geopolymer matrix, which appears to be dependent on the Si/Al ratio, and geopolymers having six different Si/Al ratios for three different curing times are also observed [23].

Fig. 2 presents high-magnification images of a geopolymer with a Si/Al ratio of 1.74, revealing more details of the geopolymer matrix and the existence of crystallites, which may have formed during the geopolymerization process. The geopolymer matrix surface appears very smooth under lower magnification, as observed in Fig. 2(a). However, many small, crystallite-like particles were observed in the geopolymer matrix as well as in the network structures that connect the geopolymer matrix, as observed in Fig. 2(b). It has also been speculated that the formation of these small, crystal-like particles in the matrix and network structures might result in the high compressive strength of these FS and SCS geopolymers. However, the formation of crystallites in the geopolymer matrix has been rarely reported in other studies [26]. Therefore, a further investigation on the microstructure and crystalline structure of these small particles has been performed using TEM to identify the crystallites and determine their crystallinity. It is expected that the crystallites in the matrix of geopolymers with higher Si/Al ratios would be C-S-H with other minor phases if we examine the XRD results in Fig. 1.

TEM analysis

Fig. 3(a) shows a typical bright-field (BF) image of

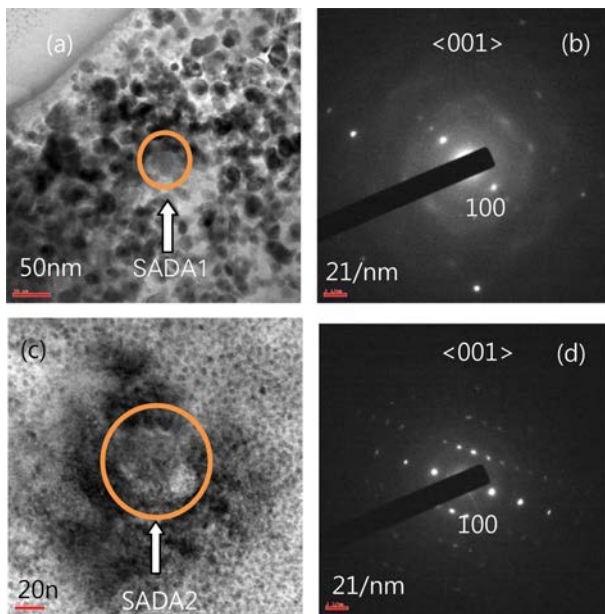


Fig. 3. TEM micrographs and SAD patterns of the geopolymer with a Si/Al ratio of 1.74 after 28 days of aging. (a) A BF image with the SAD aperture indicated by the arrow. (b) The corresponding SAD pattern from the encircled area limited by the SADA1 in (a). SAD was obtained from an area containing at least two crystallites. (c) A lower magnification BF image, which is near the area in (a), and (d) the corresponding SAD pattern from the encircled area limited by SADA2 in (c).

the geopolymer matrix of the specimens with low Si/Al ratios (0.7-1.5) after 28 days of aging. There are many small particles with sizes ranging from 10-30 nm. It is well known that such small particles are not expected to form in an amorphous material. Moreover, it is even less expected to find these crystal-like particles in FS- and SCS-based geopolymers because these types of slag are melted and fused in a melting furnace at very high temperatures (above 1500 °C). The XRD analysis demonstrated that there were no crystalline phases in the as-received FS and SCS, and thus, the raw materials were amorphous [23].

It is deduced from the above discussion that the crystal-like particles present in Fig. 3(a) may have precipitated or grown during the polymerization reaction of the geopolymer. It is also expected that these particles are crystallites with single-crystal structures. Therefore, TEM measurements were performed to determine their crystallographic structure. Diffraction pattern analysis and corresponding images from the SAD patterns are usually used to identify the crystallinity and orientation of inorganic specimens. The circle in Fig. 3(a) indicates the position of the selected area diffraction aperture (SADA), which was used to obtain the SAD pattern presented in Fig. 3(b). The size of SADA1 used to obtain the SAD patterns was 50 nm. Based on the SAD pattern, it can be observed that several diffraction patterns from at least two different crystallites are overlapping, as evidenced by the faint ring-like diffraction patterns and extra-

diffraction spots, which are normally observed in polycrystalline materials. The beam direction and the indexing of the spots are indicated in Fig. 3(b). As observed from the analysis in Fig. 3(b) the crystals were identified as C-S-H.

As observed in Fig. 3(c) a lower magnification was employed to see a larger area and to find larger single crystals. A relatively large single-crystal-like particle can be observed in the center of Fig. 3(c). This single-crystal-like particle was measured with SADA2, and the corresponding SAD pattern is presented in Fig. 3(d). The diffraction pattern in Fig. 3(d) is a typical SAD pattern for a single crystal, which has a perfect crystalline structure. Therefore, it is concluded that a single crystal with a mean particle size of approximately 80-100 nm as well as nano-crystallites with sizes of 10-30 nm grew or formed during the geopolymerization process. The beam direction and indexing of the spots are indicated in Fig. 3(d). As observed based on the analysis of Fig. 3(d), the crystals were identified as $\text{Ca}(\text{OH})_2$ crystals with a perfect single-crystal structure.

Conclusions

Geopolymers with six different Si/Al ratios were investigated using TEM and SEM. The existence of micro-crystallites was confirmed by SEM and TEM observations along with SAD analyses. TEM images revealed crystallites with a mean particle size of 80-100 nm as well as nano-crystallites with sizes of 10-30 nm that had grown or formed during the geopolymerization process. It may be speculated that the formation of these crystals and crystallites may result in the high compressive strength of the geopolymers.

Indexing of SAD patterns obtained from geopolymers was performed and enabled the identification of the compositions and orientations of the crystallites. At least two types of crystals were present in the matrix of the geopolymer. C-S-H and $\text{Ca}(\text{OH})_2$ crystallites were identified by SAD indexing, indicating that the amorphous state of the Ca and Si composition resulted in the crystal form of C-S-H and $\text{Ca}(\text{OH})_2$ after the hydration process, and these crystallites were the intermediate state of the geopolymerization or carbonation process. C-A-H and quartz phases were not observed in the TEM and SAD analyses because these phases disappeared at high Si/Al ratios, as observed in Fig. 1. The existence of $\text{Ca}(\text{OH})_2$ crystallites implies that extra strength of the specimen is expected at longer aging times because of the formation of CaCO_3 or CSH from $\text{Ca}(\text{OH})_2$ crystallites. The details of this mechanism will be investigated in future work.

Acknowledgments

This work was supported by the New & Renewable Energy Core Technology Program of the Korea Institute

of Energy Technology Evaluation and Planning (KETEP), granted financial resource from the Ministry of Trade, Industry & Energy, Republic of Korea. (No. 2015 3030050080).

References

1. C. Ferone, F. Colangelo, F. Messina, L. Santoro and R. Cioffi, *Materials* 6[8] (2013) 3420-3437.
2. X. Guo, W. Hu, and H. Shi, *J. Cons and Build. Mater.* 56 (2014) 81-86.
3. J. He, J.H. Zhang, Y.H. Yu and G.P. Zhang, *J. Cons and Build. Materials* 30 (2012) 80-91.
4. G. Habet, J.B. d'Espinose de Lacaillerie and N. Roussel, *J. Clean. Prod.* 19[11] (2011) 1229-1238.
5. P. Duxson, A. Fernandez-Jimenez, J. Provis, G. Lukey, A. Palomo and J. Van Deventer, *J. Mater. Sci.* 42[9] (2007) 2917-2933.
6. P. Duxson, J. Provis, G. Lukey and J. Van Deventer, *Cem. and Concr. Res.* 37[12] (2007) 1590-1597.
7. J. Davidovits, in "Geopolymer Institute" (Saint Quentin, 1999).
8. K. Sakkas, D. Panias, P. Nomikos and A. Sofianos, *Tunnel. and Under. Space. Tech.* 43 (2014) 148-156.
9. J. Davidovits, in "Geopolymer '88, edited" (The Institute, Compiègne, 1988).
10. A. Buchwald, H. Zellmann and C. Kaps, *J. Non-Cryst. Solids.* 357 (2011) 1376-1382.
11. P. Duxson, J. Provis, G. Lukey, S. Mallicoat, W. Kriven and J. van Deventer, *Colloids and Surfaces A.* 269 (2005) 47-58.
12. B.H.W.S. de Jong and G.E. Brown, *Geoch. et Cosm. Acta* 44[3] (1980) 491-511.
13. H. Xu and Jannie S.J. Van Deventer, *Cem. and Concr. Res.* 32 (2002) 1705-1716.
14. I. Lecomte, C. Henrist, M. Liegeois, F. Maseri, A. Rulmont and R. Cloots, *J. Eur. Ceram. Soc.* 26 (2006) 3789-3797.
15. C. Meral, C. Benmore and P. Monteiro, *Cem. and Concr. Res.* 41 (2011) 696-710.
16. M. Criado, A. Fernández-Jiménez, A. de la Torre, M. Aranda and A. Palomo, *Cem. and Concr. Res.* 37 (2007) 671-679.
17. Z. Xie and Y. Xi, *Cem. and Concr. Res.* 31 (2011) 1245-1249.
18. Z. Zhang, H. Wang, J. Provis, F. Bullen, A. Reid and Y. Zhu, *Therm. Acta* 539 (2012) 23-33.
19. W. Lee and J. Van Deventer, *Cem. and Concr.* 34 (2004) 195-206.
20. C. Kuenzel, L. Grover, L. Vandeperre, A. Boccaccini and C. Cheeseman, *J. Eur. Ceram. Soc.* 33 (2013) 251-258.
21. V. Barbosa and K. MacKenzie, *Mater. Lett.* 57 (2003) 1477-1482.
22. L. Liu, X. Cui, Y. He, S. Liu and S. Gong, *Mater. Lett.* 66 (2012) 10-12.
23. Y. Kim and J. Choi, *AES Tech. Revi. Int. J.* 1 (2014) 29-40.
24. J. Van Jaarsveld, J. Van Deventer and G. Lukey, *Mater. Lett.* 57 (2003) 1272-1280.
25. P. Chindapasirt and U. Rattanasak, *Waste Management* 30 (2010) 667-672.
26. S. Son, J. Lee, J. Lee and Y. Kim, *J. Kor. Ceram. Soc.* 45[5] (2008) 303-308.